Intensity distribution of the eight-beam case of the Si-888 reflection in backscattering geometry

Stefan Haubold*,[I], Klaus Dieter Liss[II], Rainer Hock[I], Andreas Magerl[I], Maren Lorenzen[III] and Michael Krisch[III]

[I] Lehrstuhl für Kristallographie und Strukturphysik, Universität Erlangen-Nürnberg, Bismarckstr. 10, D-91054 Erlangen, Germany
[II] Abteilung für Werkstoffphysik und -technologie, Technische Universität Hamburg-Harburg, Eißendorferstraße 40, D-21073 Hamburg, Germany
[III] ESRF, BP220, F-38043 Grenoble, France

Received April 11, 2003; accepted August 8, 2003

Multi beam diffraction / Backscattering / Eight beam case / Dynamical diffraction / X-ray diffraction

Abstract. The eight-beam case of the Si-888 reflection in backscattering has been studied by scanning the eight simultaneously excited reflections Si 888, Si 088, Si 880, Si 808, Si 800, Si 080, Si 008 and Si 000 in wavelength and two independent rocking angles. Largely different widths of the individual reflection profiles found are explained from the Ewald representation as suggested by kinematic diffraction theory. The intensity profiles demonstrate a coupling of the eight simultaneously excited wave fields as expected from dynamic diffraction theory.

Introduction

A silicon crystal brought into exact backscattering condition for the 888 reflection yields not only the forward diffracted and back scattered Bragg excitation, but six additional side reflections. All of them lie simultaneously on the Ewald sphere. Bragg's law is fulfilled for these eight reflections simultaneously:

$$2d_{hkl} \sin \theta_B = n\lambda \,, \tag{1}$$

where n represents the diffraction order, λ the wavelength, θ_B the Bragg angle and d_{hkl} the spacing for lattice planes denominated by the Miller indices hkl.

The side reflections may reduce the intensity and the wavelength selectivity of the backscattering reflection. Indirect excitations of one of the reflections by another one, called Umweganregungen, contribute to the total intensity of the excited reflection [1].

The simultaneous excitation of different Bragg reflections has to be taken into account e.g. when storing photons by successive backscattering reflections [2, 4] between two parallel crystal slices [3] or when designing a Fabry-Perot interferometer. Exact backscattering has been addressed recently by Shvyd'ko et al. [5] using sapphire, which lacks however the high degeneracy of simultaneously excited reflections – the salient issue of this paper.

Rocking scans of the sample have been performed for the backscattering condition [6]. Also, the energy of the impinging photons has slightly been varied by detuning the temperature of the beamline monochromator. The present investigation follows the intensities of the eight Bragg reflections Si 888, Si 088, Si 880, Si 808, Si 800, Si 080, Si 008 and Si 000 when performing angle-energy scans. The intensity behaviour of the backscattering reflection while exciting some (e.g. four beam case) or all (eight beam case) side reflections is of special interest.

The 8-beam geometry

In addition to the forward and back diffracted reflections 000 and 888, respectively, six further reflections are excited simultaneously at the exact backscattering point of the Si-888 reflection, i.e. when the photons of the exact backscattering energy impinge perpendicularly onto the (111) planes. The eight reflections represent the vertices of a cube in reciprocal space as shown in Fig. 1, and Fig. 2 represents the stereographic projection along the incident beam axis.

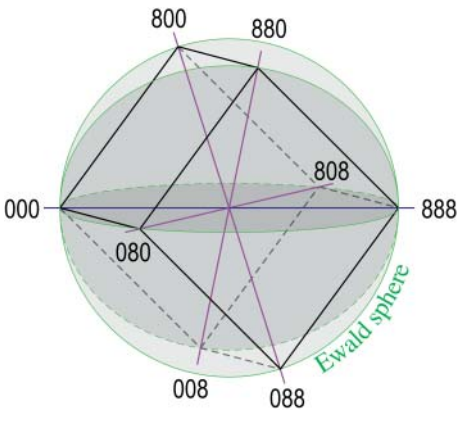

Fig. 1. The eight reciprocal lattice points corresponding to the simultaneously excited reflections lie simultaneously on the Ewald sphere. The beam impinges along the diagonal of the cubic unit cell.

* Correspondence author (e-mail: haubold@krist.uni-erlangen.de)

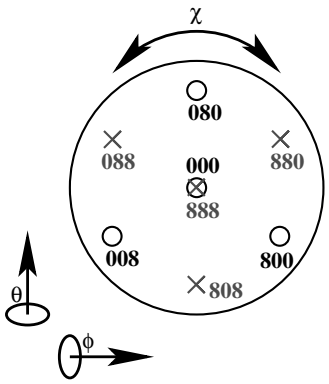

Fig. 2. Stereographic projection of the reciprocal lattice points for the eight-beam geometry, viewed against the beam. The four reflections diffracted into the backward hemisphere and into the forward hemisphere are shown by crosses and circles, respectively. This representation shows the threefold symmetry. The axes θ and φ of the angular scans are shown.

In the following we assume the φ-axis to be perpendicular to the scattering plane of the Si-080 reflection and the θ-axis to be perpendicular to both the φ-axis and the incident beam (Fig. 2).

Experiment

The backscattering instrument ID28 at the ESRF with an energy resolution of 5.5 meV and a beam divergence of about 10 μrad provides a beam with an energy of 15.8163 keV.

The photons generated by the undulators fall onto a pre-monochromator and subsequently onto a Si-888 monochromator slightly detuned from the exact backscattering condition. The beam size is limited by slits to $0.5 \cdot 0.5\ \mathrm{mm}^2$ and the photons impinge perpendicularly onto the sample mounted at an appropriate stage with three rotations for θ, φ and χ (Fig. 2).

The sample was a silicon waver of about 1 cm^2 and of a thickness of about one Pendellösungs length (283 μm). The crystal was etched to reduce distortions stemming from the cutting process, which may broaden the line widths in the scans.

A sample chamber was built including mounts for eight detectors made from avalanche photodiodes (APDs) and integrated amplifiers (Fig. 3). The eight detectors were oriented for the eight reflected beams. One of them was semitransparent and was used to register the incoming and the backscattered intensity. APDs are able to detect single photons; their maximum count rate is 10^9 cts/s.

The sample and the detectors form a rigid unit. Note, however, that the APDs with a diameter of 10 mm and mounted at a distance of 40 mm are large enough to catch the diffracted beams for all angular scans taken typically over a range of 0.2° with a step size of 1 arc second.

An important issue concerns the temperature stability: Even though the sample chamber has been evacuated for passive temperature stabilisation, the necessary stability of some 10 mK has not always been met, which necessitated occasionally a readjustment of the energy scale.

The silicon crystal was pre-aligned with the Laue method. Exact alignment was performed by an iterative procedure based on rocking scans. The energy of the photons was first chosen by some 20 meV higher than the exact backscattering energy of the Si-888 reflection, leading to two Bragg angles somewhat smaller than 90.0°. This results in two peaks corresponding to symmetric positions in a θ- or φ-scan. The exact backscattering situation is midway of the two lines. This procedure is used for θ and φ. Further, χ needs to be oriented through other reflections as a misalignment in χ couples movements in θ and φ and should therefore be avoided as far as possible.

The angle-energy scans

Wide range scans around the backscattering position of about 0.5° provide an overview of the backscattering reflection in the two-beam case. The results comply well with the expected quadratic relation for $E(\theta)$ of the kinematic approximation neglecting the coupling of the wave fields. The Taylor expansion of $E(\theta)$ at $\theta = 90°$, derived from Bragg's law, provides:

$$E(\theta) = \frac{hc}{2d \sin\theta} \approx \frac{hc}{2d} \cdot \left(1 + \frac{1}{2}(\Delta\theta)^2\right) = E_0 \cdot \left(1 + \frac{1}{2}(\Delta\theta)^2\right). \quad (2)$$

The parabolic shape of the diffracted intensities in Fig. 4 are in accordance with this formula.

The intensities of the eight reflections were simultaneously scanned in the θ-φ-space. In addition the energy of the impinging photons was varied around the critical backscattering energy E_0 by a factor 10^{-6} by detuning the temperature of the monochromator.

In Fig. 4 the intensity of the reflections was plotted in a colour-scale. The intensity of the backscattering reflection and of some excited side reflections is indirectly represented in the transmitted beam (Fig. 4a) and in the Si-080 reflection (Fig. 4b).

If one of these reflections is excited, the intensity of the transmitted beam decreases. We call one reflection shadowed by another if its intensity decreases significantly because of the excitation of the other.

In the representation of Fig. 4 the minima of the intensity caused by the simultaneously excited Si-888-backscattering reflection lie on a parabola. The sharp line at $\Delta\theta = 0°$ is due to the reflections Si 008, Si 800, Si 880 and Si 088 being much sharper in the θ-scan than the Si-888, Si-080 and the Si-808 reflections. In the upper panel the mid-point of the parabola indicates some weaker extinction visible from the lighter colour code. The observed variation of the peak intensities is related to the peak widths characterized by a pronounced increase at the vertex of the parabola. In addition a slight misalignment in energy due to temperature drifts (see section "Discussion of the reflection positions") may be a further cause for a reduced beam intensity at the vertex point. In the θ-scan the reflection Si 080 is extremely broadened and ex-

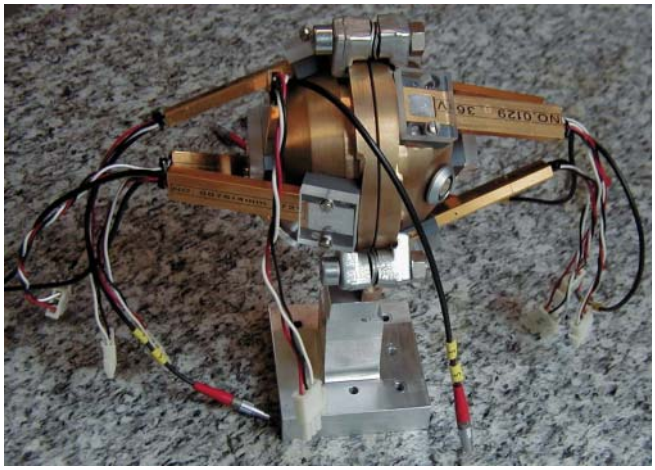

Fig. 3. The sample chamber with the APDs.

tends over the entire scan range (see section "Discussion of the reflection profiles").

Note, that scans in θ and φ of the 888 reflection become equivalent in the exact backscattering position.

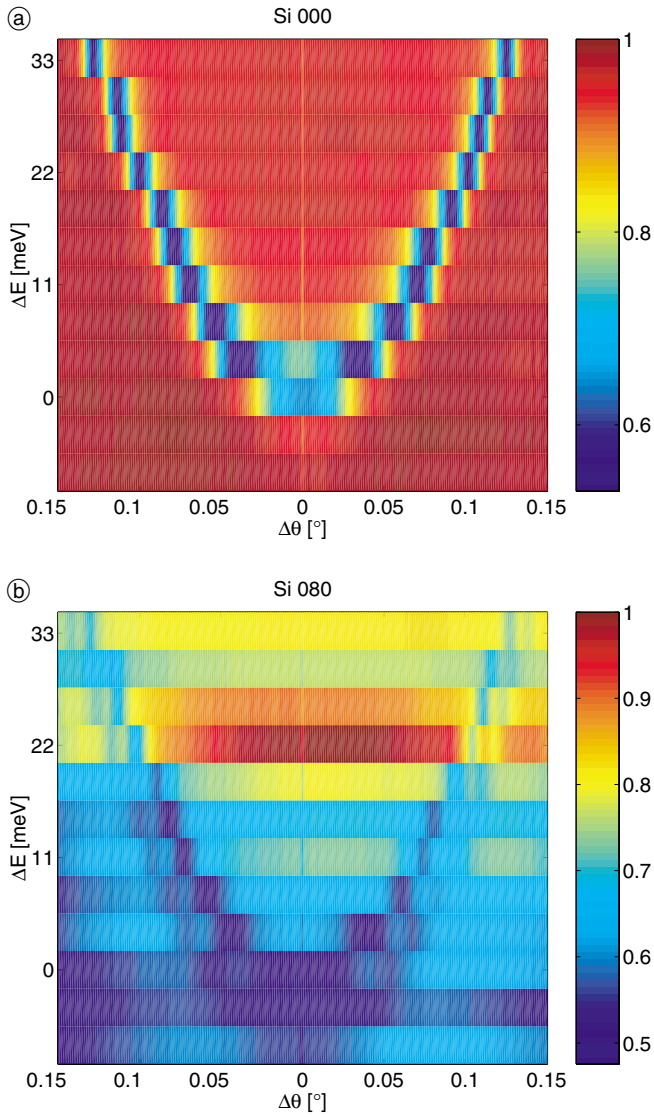

Fig. 4. Scan in the angle-energy space of the forward reflection Si 000 (**a**) and of the side reflection Si 080 (**b**).

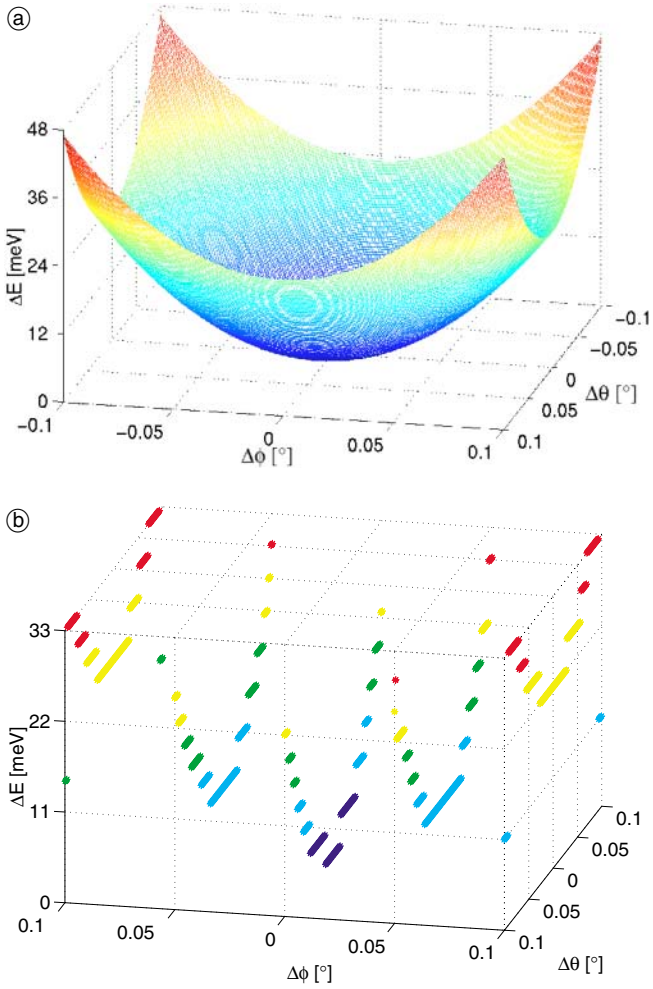

Fig. 5. The peak positions in angle-energy space of the Si-000 minimum acoording to theory (**a**) and experiment (**b**).

The reflection profiles obtained in these angular scans can be explained by cuts of the eight reciprocal lattice points with the Ewald sphere. The intensity of the forward transmitted Si-000 reflection decreases when other reflections are excited.

The Si-888 reflection is scanned with a broad line width of approximatel 200 arc seconds. This agrees with a calculated rocking width of 170″ from the Ewald construction and the instrumental energy resolution (Fig. 6) and assuming a triangular rocking profile:

$$\Delta\theta_{888} = 2\arccos\left(\frac{E_0}{E_0 + \Delta E}\right). \tag{3}$$

In contrast, the reflections 008, 800, 880 and 088 occur only in a small angular range of a few arc seconds around θ. Their widths are determined mainly by the beam divergence and the specific trajectories of the reciprocal lattice points through the Ewald sphere.

θ-scans at different φ-positions

The angular positions, the width and the excitation of the backscattering reflection depend strongly on the energy of the impinging photons. In contrast the peak positions of the side reflections do not change much with the energy

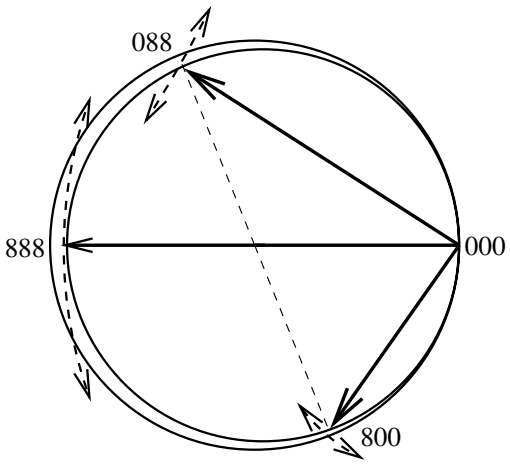

Fig. 6. The Ewald sphere cut with the scattering plane of the 800 reflection is representated with the radius vectors (some shown by dashed lines) and **q**-vectors of the four reflections lying in that plane. The finite energy resolution is schematically represented by two circles with different diametres. The widths of scanned reflections depend on the intersection angles between the Ewald sphere and the pathways described by the reciprocal lattice points during the scan.

of the impinging photons. However, they do depend strongly and linearly on θ-scans on the alignment in φ.

This observation complies with the above discussed cuts of the Ewald sphere. Any misalignment in φ leads to peaks in the side reflections not centred any more with respect to the origin. Two reflections diagonally opposite on the Ewald sphere always occur at the same position in the angle-scans because of symmetry. The peaks of the two pairs 008 and 880 as well as 800 and 088 are displaced from the origin by the same absolute value, one pair in the positive, the other one in the negative direction. This is due to the fact that the corresponding reciprocal lattice points are opposed on the Ewald sphere and turned around the same centre in the rocking scans.

Discussion of the reflection positions

Fig. 5 shows that the prediction for the position of the Si-888 reflection complies well with the experiment. However, the energy axis had to be rescaled due to a lack in temperature stability. During the scan taken over 30 hours, the temperature at the sample drifted by some 0.5 K which corresponds to an energy shift of some 18 meV leading to a correction factor of 1.5 as seen from the ordinates in Fig. 5.

The picture in Fig. 8 is obtained when marking all the positions in a θ-φ-diagram where the reflections are excited. We assume that there is no misalignment in χ. The circle in the centre becomes smaller if the energy of the photons and consequently the radius of the Ewald sphere is reduced. This is due to approaching intersection points between the Ewald sphere and the pathways described by the reciprocal lattice points in the rocking scans. If the photon energy is lower than the critical backscattering energy, the backscattering reflection disappears.

The location curves for the peaks of the side reflections intersect with an angle of 60° as a consequence of the threefold symmetry.

Discussion of the energy resolution

The width of the backscattering reflection of the monochromator in energy space is a most crucial point in backscattering instrumentation. It determines the possible energy resolution of the measurements. In practical applications the monochromator is slightly detuned from the exact backscattering position to avoid a multi-beam case deteriorating the energy resolution of the instrument [7].

Dresel [8] has given the following analytic solution for the energy resolution in a two-beam case:

$$\frac{\Delta\lambda}{\lambda} = \frac{\chi_{hkl}}{\sin^2\theta_B} + \frac{\Delta\theta}{\tan\theta_B} + \frac{(\Delta\theta)^2}{2\sin^2\theta_B}\,, \tag{4}$$

where χ_{hkl} is the Fourier component of the dielectric susceptibility and $\Delta\theta$ the beam divergence. From this follows an energy resolution of $1.7 \cdot 10^{-7}$. This complies well with the measured energy resolution of 5.5 meV considering that the measured value results from a convolution of the monochromator's and anaylzer's resolution functions. In the eight-beam case with the coupling of eight wave fields the energy resolution may no longer be calculated with this formula. The energy resolution of the side reflections 088, 808, 880, 800, 008, and 080 is worse by about one order of magnitude (within the beam divergence accepted by the side reflections), which in turn deteriorates the energy resolution of the backscattered reflection. This appears plausible assuming a higher apparent extinction

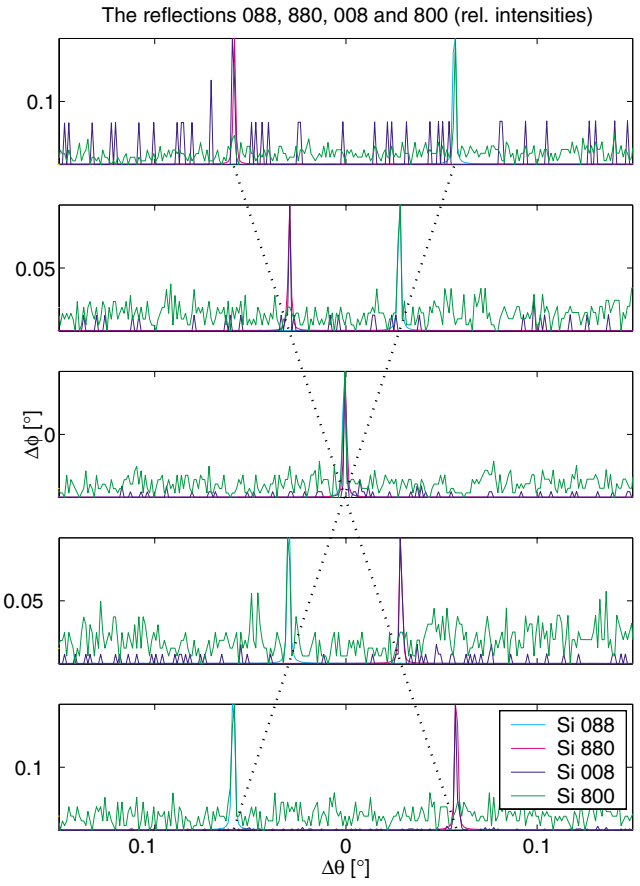

Fig. 7. θ-scans at different φ-settings for four side reflections. The lines across the panels are the location curves of the peaks.

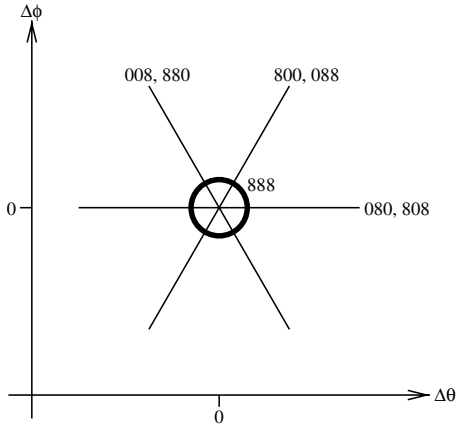

Fig. 8. Positions in the η-φ-space where reflections are excited. The diameter of the circle (888 reflection) depends on the energy of the impinging photons. If the exact backscattering energy is reached, this circle reduces to a point at the centre. Further the 000 reflection is excited at any angular setting.

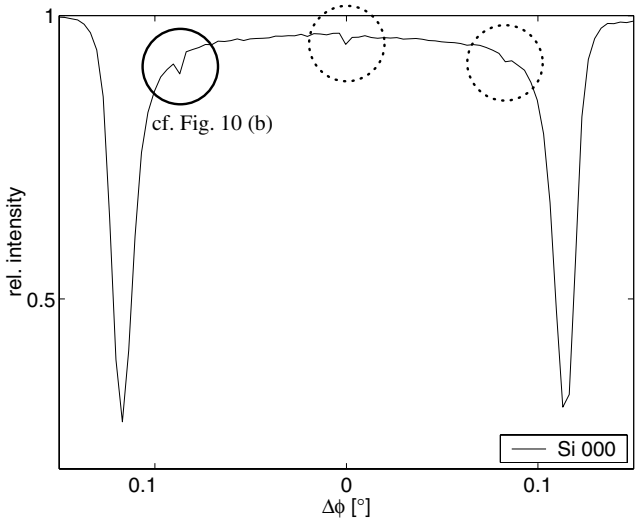

Fig. 9. Intensity profile of the transmitted beam (Si 000). The small dips occur because side reflections are excited in a four-beam case decreasing the intensity of the transmitted beam.

through the side reflections in accordance to its proper wavelength selectivity. This results in fewer lattice planes to contribute to the backscattering reflection and thus increases its width in energy space. The detailed distribution, however, is rather complicated and a complete account can only be given by theoretical consideration involving fully dynamical theory [9].

The instrument ID28 operating at 89.865°, slightly away from the backscattering position, has an experimentally determined energy resolution of 5.5 meV for the 15.8163 keV photon energy [10]. Unfortunately, this is about one order of magnitude less than used in the numeric simulations by Schwegle [9], where a pronounced fine structure in the rocking profiles can be seen. Together with the imperfect temperature stabilisation of 100 mK corresponding to 3.69 meV, the energy resolution of the instrument limits the possibilities of this setup.

The minimal divergence of the instrument is about 3 arc seconds in the vertical direction, whereas the numerically calculated Darwin widths of the examined side reflections are only about 0.1 arc seconds. This means that the recorded reflection profiles of these side reflections are dominated by the divergence of the instrument. It follows that dynamic widths and intrinsic reflection profiles of these reflections cannot be investigated with this kind of setup. A better resolution could be obtained with nested channel-cut monochromators [11].

Alternatively and in two dimensions, the necessary angular resolution in the instrumental setup could be envisaged by twisted pair monochromators where one monochromator in backscattering position provides the necessary energy resolution, whereas another pair far away from backscattering determines the necessary angular divergence.

Coupling of the wave fields

Zoomed scans reveal more details in the scanning profiles. An intensity profile of the transmitted beam (Si-000 reflection) is plotted in Fig. 9. The two pronounced dips at the edges of the scan arise from the backscattering reflection Si 888, which appears double because the photon energy is slightly higher than the exact backscattering energy.

We have looked upon the intensity of the non-excited reflections and found at this particular angular positions that some of them increase when another reflection is ex-

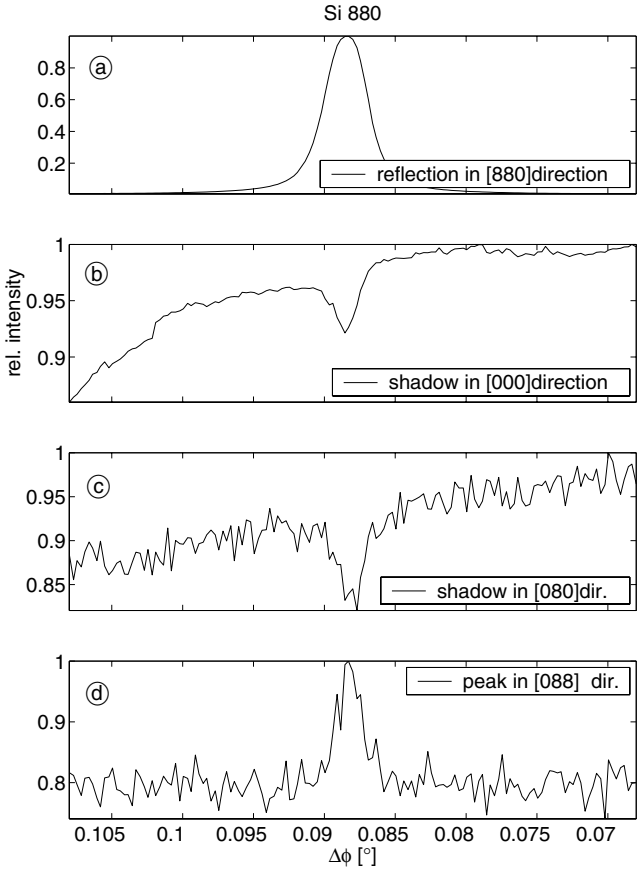

Fig. 10. Intensity profiles for some detectors taken for a φ-scan of the Si-880 reflection. The peak is shifted by $-0.088°$ because the energy and the φ-angle are slightly detuned with respect to the backscattering case. Intensities are normalized to the highest count rate of the individual scans.

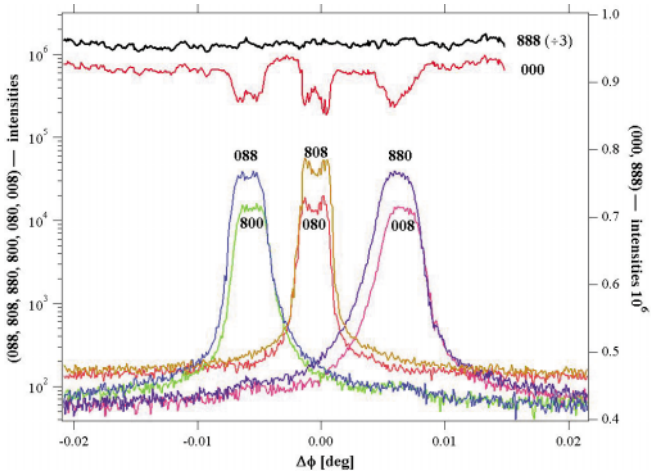

Fig. 11. Intensity profile in a simultaneous φ-scan of the eight reflections taken near the exact backscattering point $\Delta\theta = 0$, $\Delta E = 0$. The width of the reflection 888 is much larger than the present scale. Opposite reflections on the Ewald sphere appear simultaneously.

cited. The wave fields of simultaneously excited reflections in the crystal couple such that the intensity contained in each reflection may increase or decrease.

The scan in Fig. 9 has been followed up experimentally in greater detail. Fig. 10 (b) is an enlargement of the small dip on the left hand side of Fig. 9. This dip occurs at $\Delta\varphi = -0.088°$ and is caused by the Si-880 reflection. At the same time, the Si-088 reflection shows a peak at $\Delta\varphi = +0.088°$ and the Si-080 reflection at $\Delta\varphi = 0°$. In Fig. 10 the simultaneously measured intensities in the directions [000] and [080] decrease at the peak position of the Si-880 reflection referring to the φ-scan. Note that the intensity in the [088] direction increases. This demonstrates coupling between the 880 and the 088 reflection.

Consequently, exciting one of these reflections directly may increase (+) or decrease (−) the intensity of the other reflections, as noted in Table 1. In each case one reflection is excited directly and it has been followed how the intensities of the other reflections change. This is an indirect observation of the excited reflection.

Table 1. Positive (+) or negative (−) coupling of reflections.

excited reflection	kind of observation	FWHM	sign
Si 880	indirectly in Si 000	9.3″	−
	indirectly in Si 088	8.4″	+
	directly	13.2″	+
	indirectly in Si 080	8.0″	−
Si 088	indirectly in Si 000	7.2″	−
	directly	13.3″	+
	indirectly in Si 880	8.0″	+
	indirectly in Si 080	10.3″	−
Si 080	indirectly in Si 000	2.8″	−
	indirectly in Si 080	2.8″	+
	indirectly in Si 880	4.6″	+
	directly	6.5″	+
Si 888	indirectly in Si 000 at $\Delta E = 30$ meV	51.5″	−

The effect of indirect excitation may be quite annoying in structure determination because the intensities may be measured wrongly. Alternatively, indirect excitations have proven valuable for a determination of the phase problem in structure determination [12]. In our particular setup multiple excitations have the virtue to offer a useful observation method: One can detect one reflection by observing the shadow thrown onto another one, i.e. in principle information on all possible reflections becomes visible in one detector only.

Fig. 11 shows another example of coupling of wave fields. In this case, the backscattering situation has been approached so closely that the profiles of the side reflections are already penetrating into each other. There are three pairs of reflections, each belonging to two opposite reflections: 008 and 880, 080 and 808, 800 and 008, respectively. The residual peak shifts are still due to a slight misalignment in θ. The asymmetry of the peaks is due to anomalous absorption. Each pair of reflections contains a Laue and a Bragg one. The reflections in Laue geometry are less intense than their counterparts in the Bragg case. This is due to higher absorption when passing through the whole crystal thickness. Note the asymmetry and bumps in the tails of the individual curves. We relate them to the coupling of the wave fields in these angular positions.

The influence on the intensity of the backscattered reflection when other reflections are excited is to be clarified when storing photons. In a numeric simulation of the eight-beam case of Si 888 [9] the backscattered intensity even reaches its maximum value in the exact backscattering position in spite of the fact that all other reflections lie simultaneously on the Ewald sphere.

Discussion of the reflection profiles

Neglecting coupling of multiple reflections, i.e. within the frame of kinematical diffraction theory, the reflection profiles can be derived from the Ewald construction.

During the scans the reciprocal lattice points move on circular pathways around the origin 000. In this representation the energy width and the divergence of the impinging beam provides a finite width for the Ewald sphere. The intersection region between the pathways and this Ewald sphere corresponds to the width of the rocking scan profiles. These cutting volumes may in the main be described by the cutting angles between the pathways and the Ewald sphere. Assuming an energy selectivity of the instrument of 5.5 meV, this provides a FWHM for the Si-888 reflection of 170 arc seconds. Note, however, that the rocking widths of the side reflections are dominated by the beam divergence and thus cannot be estimated by this consideration.

As another example we note the large θ-rocking width of the Si-080 reflection in Fig. 3. This comes about through the tangential encounter of this reciprocal lattice point with the Ewald sphere.

Conclusions

The eight-beam case of Si 888 in exact backscattering has been measured for the first time. The reflection positions and widths obtained in various angular scans can be explained by cuts of the eight reciprocal lattice points with the Ewald sphere. For a more detailed explanation of the rocking scan profiles dynamic calculations are essential. Further structures occurring in the tails of the peaks may not be explained geometrically but require calculations of the amplitudes of the coupling wave fields. The intensities observed in angular scans show qualitatively the coupling of the reflections through interference of their wave fields.

Beam positions and rocking widths can be accounted for by a kinematical description as shown, while a quantitative analysis of the intensities requires a full treatment within dynamical scattering theory.

Schwegle [9] has shown in calculations neglecting beam divergence that the backscattered intensity reaches its maximum in the exact backscattering setting. This could not be verified in the present experiment likely due to insufficient angular resolution.

Even in our experiment with a beam divergence of some 10 μrad the backscattered intensity was high enough to let photon storage seem possible. The side reflections do not at all forestall backscattering in the exact backscattering condition, they even help adjusting with precision the sample, as they are much sharper in the angle space than the backscattering reflection. The detection of the side reflections will be rather an advantage in an alignment procedure than a disadvantage in terms of intensity loss.

For further experiments active temperature control of the sample seems essential. The passive temperature stabilisation by evacuating the sample chamber is no longer sufficient for measurements with an energy resolution in the meV range.

Acknowledgments. We kindly thank the ESRF staff for their generous support and Yuri Shvyd'ko, University of Hamburg, for providing us with the APDs.

References

[1] Renninger, M.: Röntgenometrische Beiträge zur Kenntnis der Ladungsverteilung im Diamantgitter. Z. Kristallogr. **97** (1937) 107–121.
[2] Liss, K.-D.; Hock, R.; Gomm, M.; Waibel, B.; Magerl, A.; Krisch, M.; Tucoulou, R.: Storage of X-ray photons in a crystal resonator. Nature **404** (2000) 371–373.
[3] Mitschke, M.: Unpublished results. http://www.lks.physik.uni-erlangen.de/publications/diplom/mitschke.pdf
[4] Liss, K.-D.; Hock, R.; Gomm, M.; Waibel, B.; Magerl, A.; Krisch, M.; Tucoulou, R.: X-ray photon storage in a crystal cavity. Proceedings of SPIE, 4143: 78–88, 2001, http://www.esrf.fr/exp_facilities/ID15A/science/resonator/SPIE4143–15.pdf
[5] Shvyd'ko, Yu. V.; Lerche, M.; Wille, H.-C.; Gerdau, E.; Lucht, M.; Rüter, H.-D.; Alp, E. E.; Kkachatryan, R.: X-ray interferometry with micro-electronvolt resolution. In print, Hamburg, 2002.
[6] Haubold, S.: Unpublished results. http://www.lks.physik.uni-erlangen.de/publications/diplom/haubold.pdf
[7] Krisch, M.: Private communication, krisch@esrf.fr
[8] Dresel, C.: Unpublished results.
[9] Schwegle, W. F.: Theoretische und Experimentelle Untersuchungen an Mehrstrahlinterferenzen. Master thesis, Universität (TH) Karlsruhe, 1993.
[10] Requardt, H.: Welcome to ID28, 2000. http://www.esrf.fr/exp_facilities/ID28/ID28.html
[11] Toellner, T. S.: Monochromatization of synchrotron radiation for nuclear resonant scattering experiments. Hyperfine Interactions **125** (2000) 3–28.
[12] Weckert, E.; Hümmer, K.: Multiple-Beam X-ray Diffraction for Physical Determination of Reflection Phases and ist Application. Acta Cryst. A**53** (1997) 108–143.